Dielectric Physics Approach for Improvement of Organic-Field Effect Transistors Performance

Martin Weis and Mitsumasa Iwamoto

Abstract We present a brief review on charge transport in organic field-effect transistors (OFETs), which is necessary to further design nanostructured devices. Dielectric physics is used to explain charge transport of these organic devices in the steady and transient states. We clearly show the influence of internal fields on charge accumulation and transport, and propose models for potential distributions across the OFET channel. Potential drop on the electrodes (the contact resistance) is also discussed and its control is described. Improvement of OFET performance is explained in terms of the design of device dimensions, materials and operation regime.

1 Introduction

Semiconductor devices based on organic materials [1], such as thin film transistors [2] and light emitting diodes [3], have attracted much research interest for their promising applications in various fields. With the development of organic materials with high mobilities, a recent trend in the research on the OFET has been concentrated on applied research, mostly focused on increasing carrier mobility and many experimental approaches have been exerted. Among them are the

M. Weis
Institute of Physics, Slovak Academy of Sciences, Dubravska Cesta 9,
845 11 Bratislava, Slovakia

M. Iwamoto (✉)
Department of Physical Electronics, Tokyo Institute of Technology, 2-12-1 O-Okayama,
Meguro-ku, 152-8552 Tokyo, Japan
e-mail: iwamoto@ome.pe.titech.ac.jp

Fig. 1 Simplified view of organic electronic devices: **a** OFET and **b** OSIT. The *arrows* depict charge carrier paths from the source to the drain electrodes
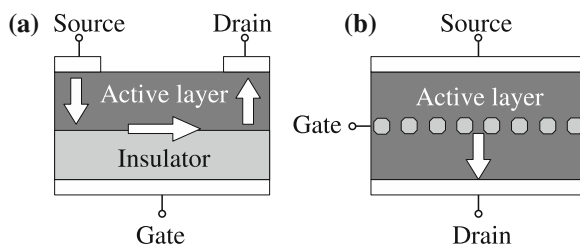
development of modified surface gate insulators and the use of a single crystal semiconductor layer [4, 5]. Along with these endeavors, basic research, such as injection, accumulation and transfer mechanisms, is being utilized to improve OFET performance. Even though there has been significant study, the device physics of OFETs is not yet clear, in comparison with that of inorganic FET structures. Various theoretical studies have been carried out to clarify the device physics of OFETs [6–8], but attention was focused on transport phenomenon only. Recently it has been shown that carriers injected from a source electrode dominate OFET operation. However, owing to the ambiguities of energetics at the organic–metal and organic–organic interfaces, device performance is not fully understood. Therefore deep understanding of injection and transport processes is crucial for further application of OFETs. It should be mentioned here that organic electronic devices are promising candidates for steady-state application and also for high-frequency devices. Therefore, improvement of device performance requires an increase in output current (for a specific applied voltage) as well as reduced response time. However, the successful design of organic device requires a suitable device model.

In contrast to inorganic semiconductors, organic materials have different mechanical, optical and, to some extent, electrical properties. However, electronic devices based on organic molecular materials exhibit similar behavior to inorganic analogies; hence, the name organic semiconductor is used [1]. On the other hand, the low charge- carrier mobilities reported by many research groups suggests classification of these materials as dielectrics, i.e., materials in which the thermodynamic equilibrium is not established. The simplest structure used for investigating material properties is represented by an organic semiconductor sandwiched between two electrodes. For a low intrinsic mobility, it is usually denoted as a metal–insulator–metal (MIM) structure. The OFET, which is most common object of study, is a planar device ruled by injected excess charges (Fig. 1a). Although OFET is well-studied in academic research, it is not widely used and its application requires further improvement. It is necessary to note that OFETs with alternative structures, like vertical OFETs [9] or organic static induction transistor (OSIT) [10], have been proposed. Here, the OSIT is based on the idea of the organic semiconductor film sandwiched between the source and drain electrodes with the gate electrode in the middle of the film (Fig. 1b). The gate electrode is usually a grid [11] or semitransparent (non-continuous) film [10] of metal with blocking contact, which reduces the leakage current. Note that

original idea of inorganic SIT lies in the regulation of slit width by controlling depletion layer with applied gate voltage. However, this situation is doubtful for organic SIT and development of new model is needed, as explained in Sect. 2.3.

Interestingly, for the various device structures reported, different models based on different physical background are used for the same organic material [8]. The MIM and OFET structures are discussed on the basis of insulators and semiconductors, respectively. In addition, due to ill-defined differences, the designation "semi-insulators" was proposed. Moreover, the charge transport in the OSIT device was not described clearly and suggested models [12] cannot explain experimental results [13]. Hence, there is a need to find an alternative model that can describe all the aforementioned structures.

2 Steady-State Current Flow

In the following discussion, the electrodes for injection and collection of the charge are denoted as a source and drain, respectively. Even though these names are commonly used for transistor devices only, they hold for the MIM structure, too, and can provide us with a better understanding of the carrier transport mechanism. In this study, the organic semiconductor is treated as a dielectric material with negligible intrinsic carrier density and a single type of charge carrier can be injected and transported (e.g., p-type conductivity). In addition, the carrier mobility μ and the dielectric constant ε are assumed constant throughout the active layer and internal field (e.g., due to dissimilar electrodes) is neglected. The current density j through the device can be described in accordance to Ohm's Law as

$$j = en\mu E \tag{1}$$

where en, μ, and E are charge density (e is elementary charge), free carrier mobility and electric field, respectively. Hence, the aim of this discussion is the proposal of an appropriate model, which can provide the charge density and average electric field.

2.1 Metal–Insulator–Metal Structure

The current–voltage characteristics are common sources of information on charge transport through MIM devices [14]. The analytical description of the charge transport is usually based on the drift–diffusion equation solved for the Poisson field [15]. However, the propagation of charges can also be solved along with the equivalent electric circuit with distributed parameters. For analysis of the structures using circuit theory, we break the problem into small parts so that the circuit element dimensions will be infinitesimal small. Thus, the parameters of equivalent circuits spread throughout the line are expressed by distributed parameters

Fig. 2 Schematic view
of MIM device and its
equivalent circuit
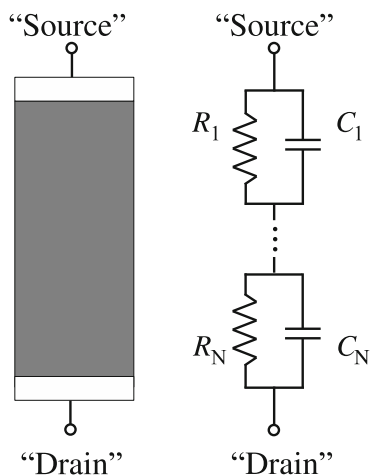
(units per unit length). Here, the equivalent circuit stems from the Maxwell's basic idea that a current flowing through the active layer is given by sum of the conduction and displacement currents. Therefore, the resistor, R, and capacitor, C, components of equivalent circuit represent these two contributions and they are connected in parallel, as shown in Fig. 2.

On the other hand, these elements of the equivalent circuit stand for the physical phenomenon: R and C illustrate the distribution of the electric field and charge, respectively. In detail, for low voltages the constant electric field, i.e., linear potential profile through dx, is modeled by a constant resistor representing potential drop across the distance, dx. Hence, the Maxwell relaxation time $\tau = RC$ for the region between injection (source) and charge collecting (drain) electrodes represent the spreading of the charge:

$$\tau = \frac{\varepsilon}{\sigma}, \tag{2}$$

where ε and σ represent organic material's dielectric constant and conductivity. The relaxation time, τ, is constant and is a material property. According to Maxwell's electromagnetic field theory, charge, Q, is accumulated at the interface between two dielectric materials with different relaxation times when current with density j flows across the two-material interface. In other words, the current density induces an accumulation of the charge in accordance with the relation:

$$\nabla \cdot D = \nabla \cdot \frac{\varepsilon}{\sigma} j = Q_s, \tag{3}$$

where D represents electric flux density and Q_s is surface charge density ($Q_s = Q/S$, where S is area). Hence, in the modeling of a MIM device by a series of RC loops illustrates a distribution of parameters appearing to be dependent upon charge accumulation. However, although the model of MIM device consists of multiple interfaces, their relaxation times are identical because of constant material

parameters, σ and ε. Thus, there is no charge stored in the device and the current density in the low electric field region is:

$$j = \sigma \frac{V}{d}, \tag{4}$$

where V is the voltage applied on the device with film thickness d.

Subsequently, in the high electric field regime, the current follows the well-known space-charge limited conditions (SCLC) [14]:

$$j = \frac{9}{8} \varepsilon \mu \frac{V^2}{d^3}. \tag{5}$$

This tendency has also been observed experimentally, which verifies the dielectric approach for MIM devices. Equation 3 suggests that charge accumulates steadily in the film while the voltage is applied, indicating the Maxwell relaxation time given by Eq. 2 is spatially changing due to injected carriers that contribute to carrier transport (see Sect. 3.1). Further noting that Eq. 2 also accounts for charge trapping in MIM devices under the assumption that the trapping time differs from the dielectric relaxation time of the active layer, ε/σ. Thus, discussion based on the relaxation time can be carried out without the loss of generality.

2.2 Organic-Field Effect Transistor Structure

In contrast to the MIM devices, where the charges are transported throughout the bulk of the active layer, the charge transport across the channel in OFET devices is limited to the active layer–gate insulator interface only [8, 16]. This charge transport mechanism induces high-carrier density at the interface, which causes the drain–source current saturation for higher drain–source voltages (Fig. 3). The potential and charge distribution across the channel is simulated by another equivalent circuit (Fig. 4). Here the current flows from the source to the drain electrode through series-connected capacitors and resistors, per unit length. Therefore Cdx and Rdx are the capacitance and resistance, respectively, across the distance dx. Note that Rdx represents the conductivity of surface of active layer and Cdx the gate insulator capacitance. In accordance with the model proposed for the MIM device, the active layer capacitance C_a and gate insulator resistance R_g are connected in parallel with the active layer resistance, R_a, and the gate capacitance, C_g. However, for the OFET electrode setup, the drain–source capacitance represented by C_a is negligible. In addition, we assume ideal gate insulator ($R_g \to \infty$). Thus C_a and R_g elements of electrical equivalent circuit are neglected.

Application of the drain–source and gate–source voltage in accordance with Eq. 2 induces charge accumulation on the active layer-gate insulator interface due

Fig. 3 The output
characteristics of pentacene
OFET [17] for various
gate–source voltages.
Open symbols represent
experimental data,
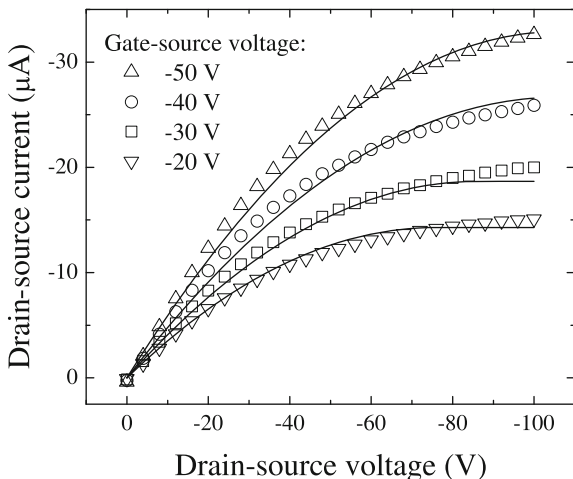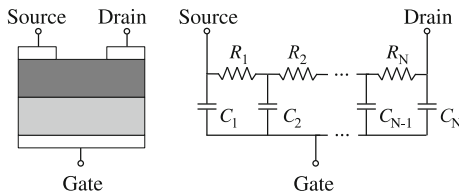*solid lines* depict
calculation result of Eq. 8

Fig. 4 Schematic view
of OFET device and its
equivalent circuit

to a discrepancy in relaxation times. Hence, the charge density, Q_s $(=en)$, is described by the relation:

$$Q_s = C_g V_{\text{eff}} = C_g \left(V_{\text{gs}} - \frac{1}{2} V_{\text{ds}} \right) \left(1 - \frac{\tau}{\tau_g} \right), \tag{6}$$

where τ and τ_g are relaxation times of active layer and gate insulator, respectively, C_g is gate capacitance per unit of area and V_{eff} is average potential voltage across the channel. To approximate the linear potential profile through the channel region, $V_{\text{eff}} = \left(V_{\text{gs}} - V_{\text{ds}} \right) x/L$, where x varies from zero to L and V_{gs} and V_{ds} are gate–source and drain–source voltages, respectively. Even with the limitation of this approximation for the saturated region [16], it is widely accepted. This assumption leads to identical resistances per unit of length across the channel. Note that although the relaxation times are again conserved, the charge Q_s is accumulated due to charge spreading on the interface, i.e., capacitors representing the gate insulator capacitance are charged through the active layer. This charge moves the electric field:

$$E_{\text{ds}} = -\nabla V_{\text{eff}} = \frac{V_{\text{ds}}}{L}. \tag{7}$$

In accordance with our previous work [16, 18] we substitute Eqs. 6 and 7 into Eq. 1 to evaluate the drain–source current:

$$I_{\text{ds}} = W Q_s \mu E_{\text{ds}} = C_g \frac{W}{L} \mu \left(V_{\text{gs}} - \frac{1}{2} V_{\text{ds}} \right) V_{\text{ds}}. \tag{8}$$

Equation 8 has a form that is identical with already derived relations [8, 18], and its fit with experimental data was reported [8, 19]. Note that Eq. 8 is derived using assumption of an ideal gate insulator, $\tau_g \gg \tau$.

It is interesting to compare OFETs with the MIM device characteristics. The drain–source current for low drain–source voltages follows Ohm's Law ($I_{\text{ds}} = C_g(W/L)\mu V_{\text{gs}} V_{\text{ds}}$), i.e., the linear region, which behaves similar to the MIM device. In this voltage region, a continuous charge sheet in the channel region is established. However, increasing the drain–source voltage over $V_{\text{ds}} \geq V_{\text{gs}}$, i.e., the saturated region, induces a limitation of the interface charge represented by the *pinch-off* position, where $V(x) = 0$ V. This spatial limitation of accumulated charges leads to a saturation of the drain–source current and follows the SCLC model, with a dependence on the square of the applied voltage. Thus, the drain–source current reaches a value of

$$I_{\text{ds}} = C_g \frac{W}{2L} \mu V_{\text{gs}}^2 \tag{9}$$

and is no longer dependent on the drain–source voltage. This is shown in an experiment (see Fig. 3), where the drain–source current is linearly proportional to the drain–source voltage at first and then, at higher applied voltages, saturates (but its value depends on the gate–source voltage). Equation 8 is suitable for modeling the device behavior (see solid lines in Fig. 3) and carrier mobility evaluation from experimental data.

In addition, although the charge transport in both OFET and MIM devices is described by Ohm's Law and SCLC, the charge in the OFET is transported along the active layer-gate insulator interface only. Hence, the charge transport mechanism is the interface charge propagation, charging of the interface due to difference in relaxation times of the active layer and gate insulator.

2.2.1 Deviation from Linear Potential Profile

As it was already mentioned in the above discussion that all common models since Shockley's famous *gradual channel approximation* [20] assume a linear potential profile across the channel region. However, there still remain questions on limits of this model and how to explain the nonlinear behavior. Electric fields across the OFET channel are crucial for device design; thus, various experimental techniques have been developed to map electric fields and potential. Interestingly, a nonlinear potential (non-constant electric field) has been reported [16, 21], as depicted in Fig. 5a. Here, the optical second-harmonic generation experiment is used to

Fig. 5 a Electric field
intensity obtained from the
second-harmonic generation
experiment (Manaka) and
b re-plotted experiment in
$\log_{10}-\log_{10}$ scale. The grey
regions represent source and
drain electrode positions
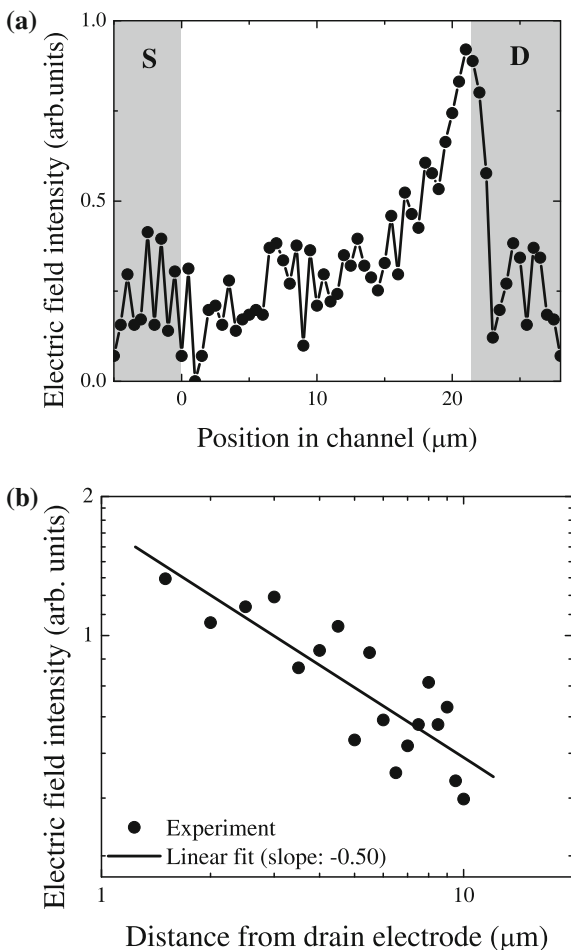
directly visualize electric field of pentacene OFET in the saturated region $\left(V_{ds} = V_{gs}\right)$.

Solving the Poisson equation is difficult if charge carriers are injected to the material. The origin of the electric field intensity distribution is influenced by various factors, such as conductive carriers, accumulated charge layer, and trapped carriers. As a result, the total electric field represents the sum of the space–charge field of conduction (mobile) carriers and the accumulated charge layer, $E_m(x) + E_a(x)$. If the contribution of accumulated and trapped charges is small, its influence on the conduction carriers can be neglected and solved independently.

Again, we can apply the concept of transmission line approximation (TLA) with distributed parameters. Here the current flows from the source to the drain electrode through series-connected circuit elements. Like before, $C dx$ and $R dx$ are capacitance and resistance, respectively (Fig. 6). The capacitance per unit of

Fig. 6 Detail view of equivalent circuit part, where after local potential $V(x,t)$ and current $I(x,t)$ are denoted
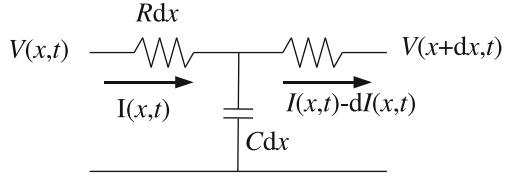
length represents the gate insulator capacitance ($C = \varepsilon_0 \varepsilon_r W / d_g$, where W is the channel width and d_g is the gate insulator thickness). For the resistance, its reciprocal value, the conductance, G, can be used as follows:

$$R^{-1} = G = en\mu\,dx = CV(x,t)\mu, \tag{10}$$

where $V(x, t)$ is the local potential, $en = CV(x, t)$. The decrease of current in the channel region due to the charging of capacitors (i.e., the creation of an accumulation layer on the active layer-gate insulator interface) can be written in the form:

$$
\begin{aligned}
-\partial I &= \frac{\partial \rho}{\partial t}\partial x, \\
-\frac{\partial I}{\partial x} &= C\frac{\partial V(x,t)}{\partial t},
\end{aligned}
\tag{11}
$$

where ρ is charge density ($\partial Q = \rho \partial x$). Simultaneously, the current flowing through the resistor decreases the potential as follows:

$$
\begin{aligned}
-\partial V(x,t) &= -I(x,t)R\partial x, \\
\frac{\partial V(x,t)}{\partial x} &= -I(x,t)R,
\end{aligned}
\tag{12}
$$

which represent the potential (carrier) propagation along the conductive channel.

The current $I(x, t)$ can be expressed in its usual way as

$$I(x,t) = en\mu\,E(\mathrm{LW}) = -CV(x,t)\mu\frac{\partial V(x,t)}{\partial x}, \tag{13}$$

where LW is channel area. Substitution of Eqs. 11 and 12 into Eq. 13 gives us

$$\frac{\partial}{\partial x}\left(V(x,t)\mu\frac{\partial V(x,t)}{\partial x}\right) = \frac{\partial V(x,t)}{\partial t} \tag{14}$$

for a gate capacitance independent of time and position in the channel. Here, the initial and boundary conditions are as follows: $V(0,t) = V_0$, $V(L,t) = 0$, $V(x,0) = 0$, which represent the applied voltage on the source and drain electrodes, and the empty channel. Because this solves for the charge propagation in the channel region, the boundary conditions of Eq. 14 represent the transport limited conditions, i.e., smooth injection with small charge carrier injection barrier. In more detail, our model does not have an element, such as diode, that represents the carrier injection process, indicating the carrier behavior after injection. In this

sense, $V(0, t)$ really means $V(0^+, t)$ and $V(L, t)$ similarly means $V(L^-, t)$, where $+$ and $-$ represent the position of electrode just inside the active-organic layer. Hence, it is necessary to note that voltage below the source electrode is equal to the applied drain–source voltage reduced by the potential drop, $V_0 = V_{ds} - V_{drop}$. Here the potential drop represents the potential difference between the source electrode and the organic semiconductor. Moreover, the potential drops illustrate the decrease in potential due to contact resistance caused by the carrier injection process from the electrode ($x = 0^-$) to the active-organic layer ($x = 0^+$). Therefore, V_{drop} represents the effect of carrier injection and can be included in our model. On the other hand, Eq. 14 is the continuity equation describing charge carrier propagation if no diffusion is present. Therefore, Eq. 14 for steady state reaches a trivial solution for a potential $V(x)$ and the electric field intensity $E(x)$ ($= -\nabla V$). $V(x)$ and $E(x)$ can be expressed as:

$$V(x) = V_0 \sqrt{1 - \frac{x}{L}}, \tag{15}$$

$$E(x) = \frac{V_0}{2\sqrt{L(L-x)}} \tag{16}$$

where V_0 is the potential below the source electrode. Distribution of the electric field is illustrated in Fig. 5a; the theoretical results are compared with experimental data. Figure 5b shows the decay of the electric field intensity near the drain electrode. A linear curve fitting shows a slope of 0.5, which indicates the field generated by conduction carriers is as described by Eq. 16. If a constant field is built across the source and drain when a steady-state current flows, then $E(0^+)$ should equal $-V_0/L$. However, according to Eq. 16, $E(0^+) = -V_0/2L$. This deviation suggests a space-charge effect caused by mobile charges in the three-electrode system.

Note that in comparison to the common SCLC electric field distribution [14], here the electric field does not vanish on the injection electrode. The reason is the propagation of mobile carriers under the aforementioned boundary conditions in the calculation, and the effect of accumulated charge is discarded, that is, $E_a(x)$ is neglected. Accumulated charge will give rise to a space–charge field, i.e., $E_a(x)$, that effectively decreases the electric field at the injection electrode and regulates the carrier injection process. Actually, as depicted in Fig. 5a, the electric field intensity is low around the injection electrode. Moreover, the field on the source electrode vanishes in the limit of channel length ($L \rightarrow \infty$); hence this model describes the influence of finite channel size in OFET.

2.3 Organic Static Induced Transistor Structure

For the OSIT devices, depending on the choice of organic semiconductor material, two different behaviors of output characteristics are reported. Generally, a diode-like tendency without presence of saturation is observed, as illustrated in Fig. 7a.

Fig. 7 The output
characteristics of an OSIT
device with active layer of
a phthalocynaine and
b BCQBT, adapted from
[23] and [13]. *Open symbols*
represent experimental data
and *solid lines* depict the
results of Eqs. 4, 5 and 19
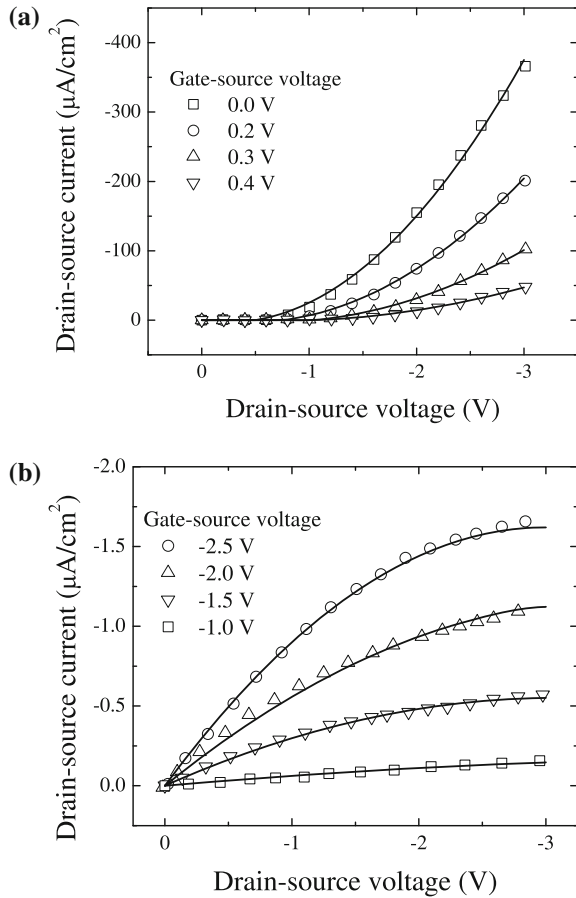
However, for some materials, OFET-like behavior with saturated current, as depicted in Fig. 7b, is typical. This discrepancy forces us to study the charge transfer mechanism in OSIT. Surprisingly, the principle of OSIT has not been discussed in detail. The theory originally proposed for inorganic SIT devices [22] is based on electrostatics and semiconductor physics, and a similar approach is discussed for OSITs [12]. Nevertheless, this approach cannot easily explain the experimental observations for different materials. This leads us to study the charge transport phenomenon in OSIT and the origin of different behaviors dependent upon the active layer material.

In accordance with our analysis, we suggest an equivalent electrical circuit depicted in Fig. 8. Here, the OSIT problem is divided into areas between (i) source and gate (ii) gate and source and (iii) the region close to the gate electrode (Fig. 8). Again, in the low electric field region, the constant electric field is modeled by a resistor representing the potential drop over the distance, dx, where x varies from zero to $d/2$ (d is the source-drain separation distance). Hence, the Maxwell

Fig. 8 Schematic view
of OSIT device and its
equivalent circuit
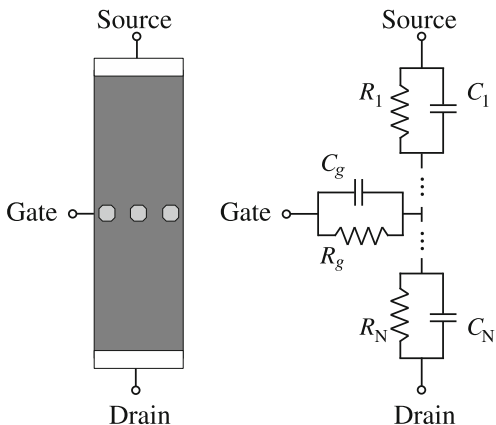
relaxation time for the region between the source (drain) and gate electrodes again
depicts the spreading of the charge in active layer. The relaxation time is constant
and a material parameter; the relaxation times $R_1C_1 = \cdots = R_nC_n = RC$ are
independent on device geometry.

The gate electrode is also modeled by its resistance and capacitance. Here, the
resistance, R_g, illustrates the leakage current ($R_g \approx V_{gs}/I_{gs}$) and its capacitance,
C_g, describes the accumulated charge on gate electrode. In other words, the
parameters R_g and C_g depend on the electrical and geometric properties of the gate
electrode; these parameters depend on the electrode type, e.g., grid or semitrans-
parent electrode, blocking contact, etc,. In contrast to the OFET device, here the
absence of gate insulator leads to a finite value of R_g.

Here, we again meet a relaxation time, $\tau_g = R_gC_g$, representing the charging of
the gate electrode region. Hence, in accordance with the solution of the Maxwell
equations for the interface of two dielectrics, the charge is stored in the capacitor
C_g only for unequal relaxation times, $\tau \neq \tau_g$. Therefore, the following discussion is
divided into two parts with respect to relaxation times.

First we discuss the case of similar relaxation times. As already mentioned, no
charge is accumulated close to the gate electrode if $\tau \approx \tau_g$. Hence, the OSIT is
simplified to the MIM structure, where the gate electrode changes the effective
applied potential V'_{ds}. In other words, the charge transport is driven by the drift of
the carriers in the source–gate field, $E_{gs} = V_{gs}/(d/2)$, and afterward in the gate–
drain field, $E_{dg} = (V_{ds} - V_{gs})/(d/2)$ (here the drain–gate voltage is evaluated as
$V_{dg} = V_{ds} - V_{gs}$). Hence, the drain–source current density, j_{ds}, is expected to
follow Eqs. 4 and 5, but using of effective applied potential V'_{ds} instead of
V. Interestingly, this ohmic and SCLC behavior is recorded in experimental data,
as illustrated in Fig. 5a by solid lines. Here we again see ohmic conductivity
($j \propto V$) in the low electric field region, $V_{ds} < 1$ V, with a SCLC behavior ($j \propto V^2$)
in the high electric field region.

Now, we will discuss the case of dissimilar relaxation times. A discrepancy in
the relaxation times of the organic semiconductor film, τ, and the gate electrode

region, τ_g, causes accumulation of charge close to the gate electrode. The amount of accumulated interface charge can be estimated by the MW model:

$$Q_s = \frac{G_g G}{G_g + G} = V'_{ds}(\tau - \tau_g)$$
$$= (C_g V_g - C_1 V_1) + (C_g V_g - C_2 V_2), \tag{17}$$

where $G = 1/R$ and $G_g = 1/R_g$ are the conductivities of the active layer and gate electrode, respectively, and V_1, ..., V_n and V_g are the potential drops throughout the resistive elements of the equivalent circuit (R_1, ..., R_N and R_g) (see Fig. 8). Assuming a low leakage current ($R_g \gg R$), we neglect the potential drop across the active layer (i.e., $V_g \approx V_{gs}$) and the accumulated charge is approximately given by the relation:

$$Q_s \approx 2C_g \left(V_{gs} - \frac{1}{2} V'_{ds} \right), \tag{18}$$

where we assumed the middle position of the gate electrode, $V_s = V_{ds}/2$, and effective drain–source voltage V'_{ds} which includes geometry effect, $V'_{ds} = (C/C_g) V_{ds}$.

Therefore, the gate electrode separating two conductive organic films limits the amount of transported charge. This phenomenon represents interface-limited current. As already discussed above, we estimate the drain–source current as:

$$j_{ds} = Q_s \mu E_{ds} = C_g \frac{2}{L} \left(V_{gs} - \frac{1}{2} V'_{ds} \right) V_{ds}. \tag{19}$$

In a high drain–source, we again see saturation of the drain–source current to a value of

$$j_{ds} = C_g \frac{1}{L} V_{gs}^2. \tag{20}$$

Surprisingly, we derived a relation almost identical with relations describing OFET behavior. The drain–source current increases with applied drain–source voltage and saturates at $V_{ds} = V_{gs}$. This result corresponds to experimental records (Fig. 7b), where saturation of the drain–source current is observed for higher drain–source voltages. Again, Eq. 12 is suitable for the modeling of device behavior (the solid lines in Fig. 7b) and the carrier mobility can be extracted.

Moreover, due to the interface charge limitation, it is expected that a drain–source current is much smaller than in case of similar relaxation constants for the case of $\tau \ll \tau_g$. This is also observable in Fig. 5, where the interface-limited current is two orders smaller than the drift current. However, a detailed discussion of the origin of the "bottleneck", the charge transport limitation, is beyond the scope of this model and strongly depends on the OSIT gate electrode preparation.

3 Charge Propagation in the Transient State

Carrier transport through the OFET as a transient phenomenon has only received attention recently [24]. The difficulty came mostly from experimental problems as well as a focus on the steady-state only. However, recently there has been research focused on the time-of-flight (TOF) method or time-resolved microscopy second-harmonic generation (TRM-SHG) technique applied to the OFET structures [24–26] and the transit time, t_{tr}, was obtained. Hence, as a first approximation, TOF analysis adapted from MIM structures was used. However, for the three-electrode system of the OFET, the charge carrier propagation can differ due to the space-charge field.

Therefore, in the following discussion, two physical models of charge carrier transport are presented and discussed separately: the MW model and the TLA. The MW model is well-known for its physical explanation of charge accumulation at the interface and relies on the electrical properties of materials. On the other hand, the TLA is common for signal propagation analysis and relies on equivalent circuits. Both models are used to explain the charge propagation in two- and three-electrodes systems represented by MIM and OFET structures. We show that both models approach to the same result. In other words, the TLA can model the charge propagation across the channel even though the conductivity distribution changes with time. A comparison of the models points out advantages as well as limitations of both evaluations.

3.1 The Maxwell–Wagner Model

Two macroscopic physical parameters characterize the organic materials used in MIM and OFET devices. These are the dielectric constant, ε, and conductivity, σ. The ratio ε/σ gives a relaxation time and represents the spreading time of the excess charge carriers in the materials. That is, a steady-state charge distribution is established after an elapsed time of around $\tau = \varepsilon/\sigma$. Note that conductivity is proportional to the carrier density n_0 and is given by $\sigma = en_0\mu$. The carrier density is generally the intrinsic carrier density of materials at thermodynamic equilibrium. According to electromagnetic field theory, the total current flowing across the organic materials is the sum of the conduction current and the displacement current. The densities of the conduction current and displacement current are given by εE and $\partial D/\partial t$ with $D = \varepsilon E$ (D is the electric flux density), respectively.

3.1.1 The MIM Device

For the MIM structures, when the injected carrier density, n, is low but is continuously supplied from the electrodes and the space–charge field caused by the injected carriers is negligible in comparison to the applied external electric field

(linear potential through the insulator), E and σE are replaced by $\sigma V/L$ and $\varepsilon V/L$, respectively. Here, L is the thickness of the insulator. This means that the MIM structure is represented merely as a parallel electrode system, $R = L/\sigma S$ and $C = \varepsilon S/L$, in carrier transport of injected carriers. We find a relationship between the time constant of the equivalent circuit, RC, and the relaxation time of the insulator ε/σ, as $RC = \varepsilon/\sigma$. That is, the time constant is free from the geometry of electrode configuration and is given only by the material parameters, σ and ε. From the equivalent circuit consideration, we find the equivalent circuit is converted into N series-connected parallel RC circuits, as illustrated in Fig. 2, suggesting the potential drop across each resistance R/N and charging of each capacitance NC must be the same, i.e., there is no charge accumulation at the connection point between segments. According to the Maxwell–Wagner effect, charge accumulation happens at the interface between two materials with different relaxation times. Hence, in an insulator represented by constant material parameters, ε and σ, there is no charge accumulation over the whole region and carriers are supplied from one electrode and are conveyed to the counter electrode across the insulator. This is actually consistent with the result of the N-series RC circuit model. The transit time of carriers across the MIM structure is given by

$$t_{\mathrm{tr}} = \frac{L}{\mu E} = \frac{L^2}{\mu V}, \tag{21}$$

and a steady-state current flows at $t = t_{\mathrm{tr}}$ after applying a step voltage, V, at $t = 0$ [14]. Obviously, we may consider this transit time gives a charge spreading time $\varepsilon/\sigma = \varepsilon/en\mu$, where n is the average carrier density of the insulator caused by injected carriers and intrinsic carriers, n_0. Therefore we obtain the relation $en = (\varepsilon V/L)/L$, representing a constant carrier distribution in the MIM after time, t_{tr}. In other words, the carrier density of the dielectric changes from n_0 to n at $t = t_{\mathrm{tr}}$.

This discussion easily extends to the case where carriers transport across I series-connected RC segments ($i < N$), i.e., from electrode to the ith connection point in the equivalent circuit shown in Fig. 2. In that situation, the time required for carriers crossing the i segments is given by

$$t'_{\mathrm{tr}} = \frac{L'}{\mu E} = \frac{L'^2}{\mu V'},$$
$$\text{with } L' = \frac{i}{N}L, \tag{22}$$
$$\text{and } V' = \frac{i}{N}V.$$

Since the charge spreading into i segments should be the same as $\varepsilon/\sigma = \varepsilon/en\mu$, we obtain $en = (\varepsilon V'/L')/L'$. That is, the carrier density of the insulator changes from n_0 to n, along with the evolution of the region of injected carriers in the presence of the electric field, E.

Therefore we may conclude that charge transport can be simply described by the drift of carriers in the average electric field, satisfying the time dependence

along the direction of the electric field. This is a sketch of carrier propagation for the case of a MIM device with two electrodes and by using TOF we can estimate carrier motion indirectly.

3.1.2 The OFET Device

The situation is quite different in the case of the OFET, a three-electrode system. As described above, at the interface between two materials with different relaxation times, charge is accumulated at the interface (the Maxwell–Wagner effect). This situation happens at the active-organic layer-gate insulator interface. The relaxation time of the gate insulator material is longer than that of the active layer, $\tau_g > \tau$. Therefore, charge is accumulated at the interface in a manner similar to trapped charges while a current flows and this situation is quite different from that of MIM, suggesting that carrier motion must be described using a model that considers interface charge accumulation.

In more detail, for the OFETs, carriers are injected from the source electrode in a manner similar to the case of the MIM structures, but they flow along the gate insulator-active layer interface in the direction from the source to the drain electrode, accompanying the interface charge accumulation caused by the MW effect. The amount of charge accumulated at the interface is regulated by the gate voltage and is given by

$$Q_s = C_g \left(V_{gs} - \frac{1}{2} V_{ds} \right), \tag{23}$$

where in the limit linear potential is built along the interface by the spreading of accumulated charge along the organic semiconductor-gate insulator interface. Here, C_g and V_{gs} are the gate insulator capacitance per unit area and the gate–source voltage, respectively. The carrier density at the active layer-gate insulator interface changes from n_0 to n, caused by Q_s. Therefore, similar to the case of the MIM structure, we can estimate the spreading time of the charge carrier at the interface. Since the carrier density is given by $en = C_g(V_{gs}-V_{ds}/2)/h$ (h is the channel thickness), the conductance along the interface is given by

$$G = en\mu \, Wh/L. \tag{24}$$

On the other hand, charge accumulation is regulated by the potential across gate insulator as described by Eq. 23, the capacitance along the channel is given by

$$C = C_g WL. \tag{25}$$

Hence, the response time is given as C/G and represents a carrier transit time, t_{tr} across the interface from the source to drain. That is,

$$t_{tr} = \frac{L^2}{\mu\left(V_{gs} - \frac{1}{2}V_{ds}\right)}. \tag{26}$$

We should note that the t_{tr} is also valid for the case when $V_{ds} = 0$ V and represents the charge accumulation condition at the interface only. Hence, it is reasonable to say that the interface charge propagation process regulates the transit time of OFETs. Furthermore, we should note that in the derivation of Eq. 23, we did not assume $|V_{gs}| \gg |V_{ds}|/2$, as in the most simple case, but the above discussion can be simplified without loss of the underlying physics [18]. In addition, although this analysis is based on a commonly-used steady-state potential distribution across the channel, it can be extended to the time-dependent accumulation of charges at the interface.

It is instructive to note that this situation can be modeled using the equivalent circuit shown in Fig. 4, where the resistance corresponds to the conductance, G, along the channel and the capacitance represents the capacitance, C, of Eq. 25. There, the potential distribution along the channel is considered and the equivalent circuit is extended to a ladder model. The transmission line model is based on this equivalent circuit, as will be discussed in following section. Furthermore, we note that in derivation of Eq. 21, we assumed the carrier injection to the interface is only from the source electrode, but t_{tr} should be reduced in case when carrier injection is also allowed from the drain. For instance, t_{tr} should be half of the t_{tr} in Eq. 21 when $V_{ds} = 0$ V instead of $V_{ds} = V_{gs}$ and we use similar electrodes as the source and drain.

3.2 Transmission Line Approximation

3.2.1 The MIM Device

The TOF method was originally designed for metal–semiconductor–metal (MIM) structures [27–29], where the carrier transport in the two-electrode system can be described as a one-dimensional problem (see Fig. 2a). Interestingly, the propagation of charges can also be solved using an equivalent circuit with distributed parameters. The equivalent circuit stems from Maxwell's basic idea that a current flowing inside a material is given by the sum of conduction and displacement currents. R and C represent these two contributions, respectively. On the other hand, these elements stand for physical phenomenon: a network of R's and C's illustrates the distributions of electric field and charge. In detail, a constant electric field (i.e., a linear potential through the semiconductor part of the MIM structure) is modeled by equal resistors representing a potential drop per distance, dx. In this model, the charge propagates from one electrode with area, S, to the opposite electrode situated a distance, d, through the resistors and the charge carrier distribution is depicted by the capacitors, C. Here, it is assumed that there is no electric field inside a metal electrode ($C_{metal} = 0$) and there is negligible metal resistance compared to semiconductor ($R_{metal} = 0$). Hence, if e and n are the elementary charge and carrier density, respectively, the distributed conductance σ can be estimated from the current density as follows:

$$j = en\mu E = \frac{CV}{d}\mu\frac{V}{d} \tag{27}$$

and by the differentiation of the current density with respect to E, defined as $\sigma = \partial j/\partial E$. Subsequently, the distributed resistance $R = d/(S\sigma)$ also extracted:

$$R = \frac{d^2}{CS\mu V}. \tag{28}$$

Although excess mobile charges are injected into the device, in this evaluation it is assumed that the effect of a space–charge field is negligible. That is why we derive the σ using $en\,E$, not the last term of Eq. 27. Thus, the electric field across the MIM structure is constant, $E = V/d$. If a voltage pulse with an amplitude, V, is applied to the electrodes, the transit time, which is represented by the relaxation time of the semiconductor in the MIM structure, can be simply estimated by the relation $t_{\mathrm{tr}} = RC$ and therefore:

$$t_{\mathrm{tr}} = \frac{1}{\mu}\frac{L^2}{V}. \tag{29}$$

Note that here the product of RC represents the relaxation of the injected carriers, and $t_{\mathrm{tr}} = RC$ with $R = \Sigma R_i$ and $C = \Sigma C_i$ (and $R_i = R_j, C_i = C_j$ for all i, j) represents the carrier transport time across all RC segments illustrated in Fig. 2. In limit of infinitesimally small elements, the sum is replaced by the integration with identical results. As such, the transit time of Eq. 29 expresses the situation where the charge carriers are conveyed through a series of RC segments in the whole MIM structure. This is described by the transit time's dependence on the voltage and the film thickness. Since there is no difference between the relaxation times of RC loops, no excess charge (like trapped charge) is stored between the segments. In more detail, the R of Eq. 28 is defined considering injected mobile carriers. This means that all charge carriers are transported across the MIM structure, even though they contribute to the space-charge field formation. The presented model with distributed parameters describes this situation, and accounts for no charge accumulation corresponding to charge trapping in the insulator layer in the MIM structure [18]. Therefore, the charge transport can simply be described by the drift of carriers in the average electric field. Furthermore, Eq. 29 suggests that the carriers will propagate with the square root of time in a drift field along the direction of the electric field intensity. In summary, we conclude that the transit time is dependent on the geometric parameter as well as the applied voltage. In the following text, we discuss the case of the OFET structures and derive the transit time.

It is instructive to note that in the state of the thermodynamic equilibrium, the dielectric relaxation time, defined by RC, is a material parameter defined by ε/σ, where ε and σ are the dielectric constant and conductivity, respectively. The dielectric relaxation time becomes independent of the geometric parameter as well as the applied voltage. Here, σ is proportional to the product of carrier density in equilibrium state ($n = n_0$) and mobility, μ. We should note that n_0 is different from

that defined in Eq. 27 due to the presence of injected carriers, $n = CV/d$. Hence, the value of RC for MIM structures and OFETs should be the same.

3.2.2 The OFET Device

The electric field propagation along the channel in an OFET (Fig. 4) was recently modeled by the TLA [16]. The TLA is based on solving the equivalent circuit consisting of infinitesimally small resistors and capacitors connected in series as a ladder. In this model, charges propagate through the channel at the semiconductor-gate insulator interface. Therefore, again, the resistance and capacitance are related to the distributions of the electric field and accumulated charge ($\rho(x) = C\partial V(x)\mathrm{d}x$). In other words, the successive charging of the capacitors represents the migration of charge carriers and resistors describe the potential drop across the channel. Note that in the presented model of the three-electrode system (OFET structure), we do not assume the influence of injection properties, i.e., the potential drop due to an injection barrier, which causes insufficient charge accumulation. Also, the displacement current between the source and drain electrodes is assumed negligible by taking into account the electrode size and separation used in this experiment. In summary, with consideration of the device parameters, the parallel segmental capacitance, found in the equivalent circuit for the MIM structure and employed to express carrier transport as displacement current, is discarded in the equivalent circuit for the OFET channel. Furthermore, since the conductivity of the gate insulator of our OFET device is extremely low, the parallel resistance element to express the carrier transport across the gate insulator is omitted from the equivalent circuit.

In the following text, analogous to the analysis of the MIM structure, the charge transport can again be solved by the relaxation times of the RC loops with distributed parameters, after calculating R in the manner we derived (Eq. 28). In the linear region (the drain–source voltage is smaller than the gate–source voltage, $|V_{\mathrm{ds}}| \ll |V_{\mathrm{gs}}|$), the constant electric field condition should be satisfied and all resistors of the equivalent circuit have identical values. Therefore, the transit time can be written as a product of the channel resistance, R_{ch}, and capacitance, C_{ch}, i.e., $t_{\mathrm{tr}} = R_{\mathrm{ch}}C_{\mathrm{ch}}$. The drain–source current I_{ds} can be expressed [8, 30] as Eq. 8. However, in contrast to the small signal analysis, here we apply a large signal that propagates across the channel. In other words, charges carry the electric field and therefore the voltage drop varies with charge carrier (i.e., potential) distribution. Therefore, the channel resistance is not constant anymore and depends on time and position, i.e., $R_{\mathrm{ch}} = R_{\mathrm{ch}}(x, t)$. For a linear approximation of the potential distribution between the source electrode edge ($x = 0$) and the charge carrier sheet edge in the channel region ($x = x^*$) is derived:

$$R_{\mathrm{ch}} = \frac{V_{\mathrm{ds}}}{I_{\mathrm{ds}}} = \frac{x^*}{C_g W \mu (V_{\mathrm{gs}} - \frac{1}{2}V_{\mathrm{ds}})}. \tag{30}$$

The channel capacitance follows:

$$C_{ch} = C_g WL. \tag{31}$$

Therefore, the transit time can be written as a product of Eqs. 29 and 30 in the form:

$$t_{tr} = \frac{1}{L} \int\limits_0^L R_{ch} C_{ch} dx^* = \frac{1}{2\mu} \frac{L^2}{V_{gs} - \frac{1}{2} V_{ds}}. \tag{32}$$

It is interesting to note that an identical result from the definition of group velocity can be also obtained:

$$v_g = \frac{dx}{dt} = \mu E. \tag{33}$$

Here, we assume a linear potential profile, $E = V'/x^* (\text{for } x \leq x^*)$ or $E = 0 \,(\text{for } x > x^*)$, with an effective voltage, V'. Trivial integration of Eq. 33 for $x \in (0, L)$ and $t \in (0, t_{tr})$ provide us with a simple relation:

$$t_{tr} = \frac{1}{2\mu} \frac{L^2}{V'}. \tag{34}$$

Note that the MW model and TLA give identical result for the MIM structure (see Eqs. 21 and 29). On the other hand, the transit time estimated by MW model (Eq. 26) and TLA (Eq. 32) differs by factor 1/2. This deviation has its origin in time-dependent conductivity, which reflects the changes of the electric field during the charge propagation. In addition, this confirms the trivial analysis of the transit time, Eq. 34.

Also, it should be pointed out that the electric propagation field is transient in an OFET. In contrast to the MIM case, where the electric field was conserved during the charge propagation, here the field depends on the position of the carrier sheet front edge ($E = V'/x^*$ (for $x \leq x^*$)). Hence, the electric field evolves in time with respect to the charge location. This is clearly illustrated in the electric field visualization prepared by the TRM-SHG technique [31, 32] (Fig. 9a). The electric field obtained from the TLA model presented for comparison (Fig. 9b).

As mentioned above, we reached the same conclusion starting from the MW and TLA models. One of the important findings from these two approaches is that the transit time, defined by Eqs. 25 and 30, is valid even when $V_{ds} = 0$. This suggests that interface charge propagation regulates transient carrier transport in the OFET channel. In the following discussion, we show such a situation by visualizing the transient electric field.

Figure 10a shows a typical transient electric field imaging at various delay times under $V_{gs} = V_{ds} = -100$ V. With an increasing delay time, the electric field moves from the source to the drain electrode and represents the edge of the carrier sheet [26]. Here, it should be noted that the electric field edge position versus the measured time on a $\log_{10} - \log_{10}$ scale reveals a time dependence proportional to the square root of time (a linear fit with slope of 0.47).
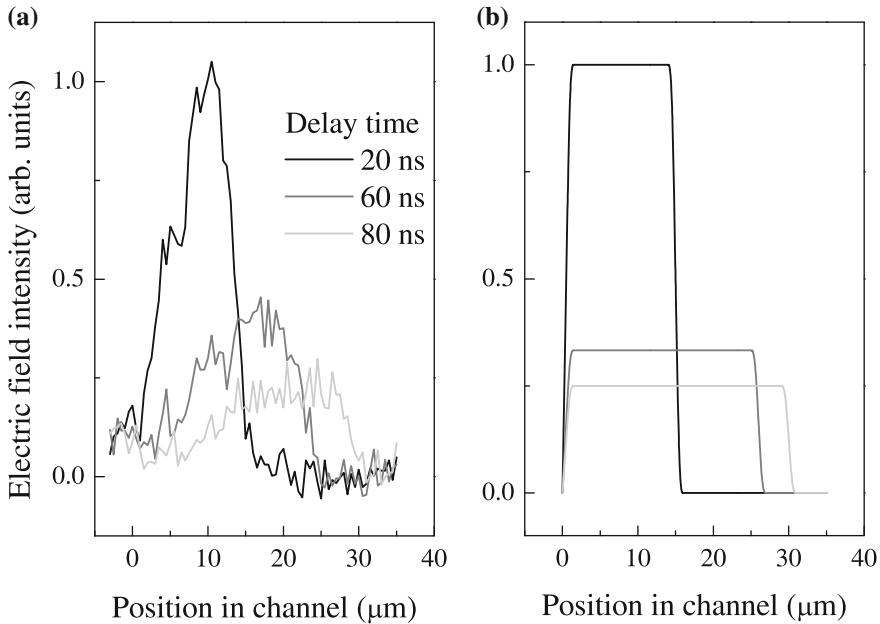
Fig. 9 Time evolution of the transient electric field propagation across the OFET channel for three different delay times, t, after application of voltage pulse ($V_{gs} = V_{ds}$): **a** TRM-SHG experiment [32] and **b** ideal theoretical case

Note that the carriers are predicted to migrate through the device proportionally to the square root of time ($x \propto t^{1/2}$). This result is in accordance with the experimental data shown in Fig. 10. However, our calculation also has other important consequences: (i) the charge is propagating through the OFET channel not only due to an electric field between source and drain electrodes, but also because of an interface charging phenomenon, and (ii) the charge is redistributing and accumulating within the channel even when no drain–source voltage is applied. In detail, in the three-electrode system, we found a different mechanism for carrier transport. In contrast to the two-electrode system represented by the MIM structure, where the transport mechanism is limited by charge carrier drift in the electric field, in the three-electrode system the charge is transported due to the propagation of interface charges (i.e., propagation of the accumulated charge layer). In other words, in the MIM structure with a single layer of dielectric material (organic semiconductor), carriers are transported directly in the direction of the electric field. On the other hand, in the OFET structure, a two-layer system (organic semiconductor and gate insulator), charge transport is due to the charging of the semiconductor-gate insulator interface and carrier motion is nearly perpendicular to the external gate field [26]. Note that the motive force, which conveys carriers within the channel, is due to the local electric field generated by injected excess charges. The lateral component of local electric of the excess charges causes a

Fig. 10 Time evolution of the transient electric field propagation in the pentacene OFET channel for different delay times t after application of voltage pulse of $V_{gs} = -100$ V and **a** $V_{ds} = V_{gs}$ and **b** $V_{ds} = 0$ V
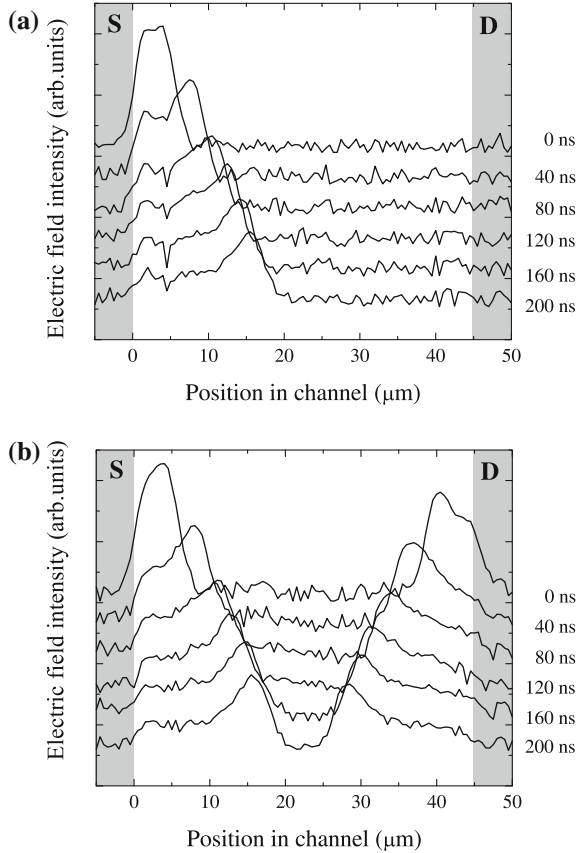
redistribution and migration within the channel toward the steady-state condition. Additionally, interface charging, which is very similar to carrier trapping but originally caused by the MW effect between the semiconductor and gate insulator layers [18], is a characteristic phenomenon originating in the OFET system. Although carrier migration through both configurations (i.e., $V_{ds} = V_{gs}$ or $V_{ds} = 0$ V) follows the square root of time law the physical reason is different. This conclusion is in accordance with the electric field visualization experiment, the electric field of the injected carriers migrates when the source and drain electrodes have the same potential (are electrically shorted, i.e., $V_{ds} = 0$ V), see Fig. 10b. The electric field records also show that the charge migration starts out symmetrically from either electrode toward the channel center due to the absence of a directional drift force between source and drain. As observed from Fig. 10, carriers migrate from both source and drain electrodes similarly. Moreover, analysis of the carrier sheet migration again shows a proportionality to the square root of time. Here we must point out that, although no drift field between source and drain electrode is established, carrier propagation is not related to the diffusion

process, which is significantly slower in organic semiconductors. Intriguingly, this experimental study is in agreement with the proposed carrier transport based on interface charging, whereas the carrier drift approach contradicts this result.

Additionally, we can discuss the relation with the Maxwell–Wagner (MW) model. Recently, the MW model was used to evaluate the pentacene-gate insulator interface under the source electrode [33, 34]. In the MW model, contact resistance has been treated by a relation for charge transport similar to Eq. 32. However, the meaning is different; the MW model describes the steady-state and is based on the presence of an interface charge caused by an electric field across the interface and a difference in relaxation times, whereas the TLA model explains charge propagation in the channel region and does not require contact resistance.

Note that a model for pentacene film with distributed R and C elements (see Fig. 4), a simple resistance R can be used instead. However, in this case the relaxation times of all repeat units (RC loops) are identical; thus, no charge is accumulated in the pentacene film, unlike the case of the MIM device. Nevertheless, the charge is accumulated at the pentacene-gate insulator interface due to the MW effect and this interface charging is in conjunction with charge transport. Therefore, the proposed TLA model describes a more realistic situation in comparison with the standard steady-state MW model, where at first charge is accumulated according to the MW effect and transported thereafter. However, we must point out that also the MW model can be extended to the case of time-dependent fields with the same result as TLA because the MW effect always causes charge accumulation at the interface between two different materials with unequal relaxation times, without a time dependence on the fields. Curiously, the transit time through the OFET device is also the relaxation time of the investigated device. In other words, the charging of the OFET represents how charge is transported in a three-electrode system.

4 How can we Improve Device Performance?

As discussed above, application of organic electronics devices requires various device properties, like thermal and temporal stability, low-cost fabrication, high output current and fast response. Even though material research and chemical engineering can provide cheap and stable organic semiconductors, device design requires understanding of underlying physics. Following discussion concludes consequences of device models and suggests road map for device improvement.

4.1 Charge Accumulation

The above analysis of an OFET based on the MW model pointed out importance of the charge accumulated at the organic semiconductor-gate insulator interface. It was shown that amount of accumulated charge is proportional to

the drain–source current. Hence, the main aim of various new device designs is increasing the accumulated charge, Q_s. Although the most common case is the enlargement of the gate insulator capacitance, it is not only opportunity for improvement. To recapitulate the possible ways, we follow a modified Eq. 6 as follows:

$$Q_s = C_g V_{eff} = C_g \left(V_{gs} + V_{dip} - \frac{1}{2} V_{ds} \right) \left(1 - \frac{\tau}{\tau_g} \right), \qquad (35)$$

where V_{dip} is potential change due to internal fields. As a result we find three different methods to increase the accumulated charge:

1. Gate insulator capacitance,
2. Internal fields, and
3. Relaxation times.

In detail, the first way is based on increasing the gate insulator capacitance ($C_g = \varepsilon_0 \varepsilon_r / d_g$) by changing its dielectric constant (ε_r) or reducing the insulating film thickness (d_g). The second way of improvement employs modification of the internal fields. This usually involves modification of gate insulator by self-assembled layers with electrostatic dipoles [35, 36], or gate insulator films with dipoles [37]. Note that the internal field has other contributions, e.g., trapping charges; thus, the total internal field is created by the superposition of all components. Interestingly, the latest way for raising accumulated charge includes the organic semiconductor properties. In other words, appropriate selection of organic semiconductor dielectric constant and conductivity with respect to the gate insulator leads to a higher accumulation of charge at the interface.

4.2 Charge Transport

After the charges accumulate at the organic semiconductor–gate insulator interface, charge transport becomes crucial for device performance. Note that this is true not only for the current's magnitude, but also for the response time, represented by the transit time. Recently, improvements of organic semiconductor mobility have achieved a level comparable to that of amorphous silicon and have brought the OFET closer to commercial applications. However, there are still other ways to reduce of the transit time. It is instructive to note that the transit time has a direct impact on the drain–source current:

$$I_{ds} = \int_0^{V_{ds}} \frac{C_{ch}}{t_{tr}} dV = C_g \frac{W}{L} \mu \left(V_{gs} - \frac{1}{2} V_{ds} \right) V_{ds}. \qquad (36)$$

That is, the total charge accumulated in the channel region is transported in time t_{tr}, i.e., $I_{ds} = Q_s/t_{tr}$. Therefore, improvement of the charge transport stands for a reduction of the transit time. In accordance with the above models, the transit time is influenced by:

1. Carrier mobility,
2. Channel length, and
3. Applied voltage.

The carrier mobility is a material parameter that depends on the organic semiconductor and the preparation technique. Note that although it is microscopic parameter related to charge transport on the molecular level, the macroscopic measurements estimate the effective value, which includes additional effects like traps and potential drops. Thus, the rise of carrier mobility depends mostly on the progress of material science and engineering.

More interesting is reduction of the channel length. The quadratic dependence of the transit time on the channel length gives us a powerful tool to reduce the response time and increase the current. This inspired researchers to design the vertical channel OFET [9] and OSIT devices. However, reducing the channel length decreases the amount of accumulated charge and the space-charge field. In other words, in the case of OSIT, the gate electrode capacitance becomes smaller than the capacitance of the source and drain electrodes. As a result the OSIT device losses its transistor behavior. Thus, the channel length reduction is limited by the preparation techniques available and the vanishing space–charge field [23].

4.3 Contact Resistance

Improvement of the carrier transport in OFETs revealed another bottleneck: charge injection. This barrier is expressed by the contact resistance, R_c, and in OFETs, it is a serious problem for practical applications [38]. The contact resistance has many origins, such as the non-uniformity of organic semiconductors, the presence of dipole layers at the metal-organic interface, electrode resistance and the interfacial energy states [39, 40]. Note that the device contact effect influences the device operation conditions, such as the potential distribution across the OFET channel [21]. The carrier mechanism is influenced by the R_c at the metal-organic material interface when the energy difference between the Fermi level of metal electrode and the highest occupied molecular orbital (HOMO) of organic semiconductor dominates the hole injection. This understanding gives us a powerful tool for contact resistance engineering. Hence, we present a brief summary of possible approaches to modify the contact resistance.

As mentioned above, the contact resistance for a specific organic semiconductor depends on the Fermi energy of electrode metal. Hence, fine-tuning the interface energetics plays a key role for smooth carrier injection. Rough adjustment of the injection barrier can be accomplished through selection of an electrode metal with

a work function similar to HOMO level (for hole injection) [41]. However, the effective work function of metal can also be changed. It was shown that exposure to the UV and ozone is helpful for surface cleaning [42], which lowers the work function [43]. Moreover, this treatment creates metal oxides on the electrode surface and thus increases the work function. Here, it should be noted that for UV/ozone surface cleaning, a decrease [42] and an increase [44] of injection barrier were both reported. Unfortunately, this simple change of the injection barrier can only be applied to bottom-contact OFETs, where the electrode is formed prior to the organic semiconductor film deposition.

Another common approach to modify injection properties is introducing a dipolar layer. Usually, a self-assembled monolayer (SAM) is created on metal-organic interface in a bottom-contact OFET [45] or on the gate insulator surface for top-contact OFET [46]. In the case of SAM grown on the electrode surface, the injection barrier is changed by the interfacial dipole [45]. In other words, the electric field of the dipole can decrease the injection barrier due to the Schottky injection mechanism. In a similar way, the SAM grown on the gate insulator surface induces a field in the organic semiconductor film and metal/organic interface [46]. However, surface modification of the gate insulator has a great effect on the crystallinity of organic semiconductor [4]. An increase of the grain boundaries (i.e., decreasing grain size) is related to the rise of trapped carriers due to interface traps and grain boundary resistance [47]. Trapped (immobile) carriers are an additional source of the electric field, which compensates the applied electric field. As a result, the contact resistance increases together with the amount of traps. A similar effect was also reported for traps at the metal-organic interface of a top-contact OFET [48].

These studies drive us to include, in the field, all excess charges in the device. A high density of injected carriers accumulated on the organic semiconductor–gate insulator can induce a local field. In more detail, an electric field, E_i, induced on the injection electrode (source) is proportional to the potential drop, V_i, created by the charge, Q_i, situated on the gate insulator surface as follows:

$$E_i \propto \frac{Q_i}{C_{\text{si}} + C_{\text{di}} + C_{\text{gi}}} \frac{1}{d} \approx \frac{Q_i}{C_{\text{si}} d \left(1 + C_{\text{gi}} / C_{\text{si}} \right)}. \tag{37}$$

Here, the capacitances C_{si}, C_{di} and C_{gi}, are related to the induced electric field on the source, drain and gate electrodes, respectively, and d is the thickness of the organic semiconductor. Therefore, detailed evaluation of the electric field effect requires charge integration across the channel. However, for a simplified problem when charges below the source electrode are considered, only the induced electric field decreases with an increasing film thickness. Figure 11 depicts an example of the voltage dependence of the contact resistance for three different film thicknesses. It is obvious that an increase of film thickness increases the contact resistance. Moreover, in case of injection slower than charge transport from the source to the drain electrode, charge accumulation is not fully established and the potential drop increases, i.e., the contact resistance rises. Note that in a

Fig. 11 Voltage dependence of the contact resistance for three selected organic semiconductor film thicknesses [50]
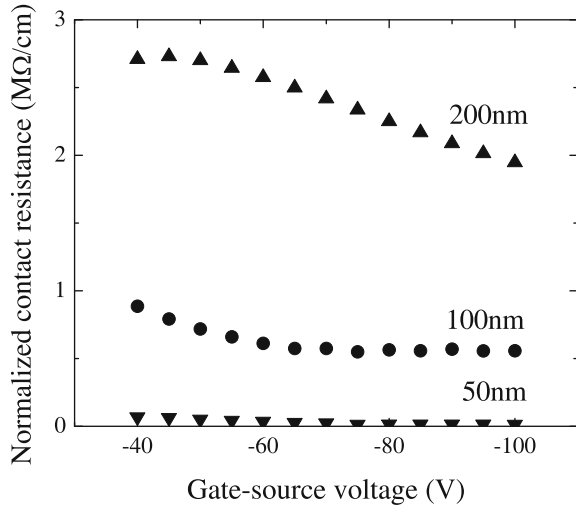
bottom-contact OFET, the charge cannot be accumulated below the electrode and contact resistance is minimized. In summary, a weak electric field's influence on the contact resistance for this device geometry was reported [49].

5 Concluding Remarks

In this brief summary we explained OFET models based on dielectric physics. Two different models were employed to discuss the charge propagation along the organic semiconductor-gate insulator interface. The MW model provides deep physical insight to the charge accumulation phenomenon and the discussion based on TLA is more suitable for charge propagation in the channel region with a variable electric field. In other words, the device can be explained by the MW charge accumulation and propagation, where charge transport is realized by the accumulation of charge on the organic semiconductor–gate insulator interface. The steady-state and transient state were explained separately to point out the importance of charge accumulation and transit time. This was later employed for device design and the improvement of device performance; possible methods were discussed and compared with each other. Hence, it results to the road map for device performance improvement.

References

1. Katz HE (1997) Organic molecular solids as thin film transistor semiconductors. J Mater Chem 7:369–376

2. Sirringhaus H (2005) Device physics of solution-processed organic field-effect transistors. Adv Mater 17:2411–2425
3. Tang CW, VanSlyke SA (1987) Organic electroluminescent diodes. Appl Phys Lett 51:913–915
4. Kim C, Facchetti A, Marks TJ (2007) Polymer gate dielectric surface viscoelasticity modulates pentacene transistor performance. Science 318:76–80
5. Knipp D, Street RA, Völkel A, et al (2003) Pentacene thin film transistors on inorganic dielectrics: Morphology, structural properties, and electronic transport. J Appl Phys 93:347/1–347/9
6. Tecklenburg R, Paasch G, Scheinert S (1998) Organic FET Current characteristics: extraction of unusual field dependences of hopping mobilities. Adv Mater Opt Electron 8:285–294
7. Zaumseil J, Baldwin KW, Rogers JA (2003) Contact resistance in organic transistors that use source and drain electrodes formed by soft contact lamination. J Appl Phys 93:6117/1–6117/8
8. Horowitz G (1998) Organic field-effect transistors. Adv Mater 10:365–377
9. Uno M, Tominari Y, Takeya J (2008) Three-dimensional organic field-effect transistors: charge accumulation in the vertical semiconductor channels. Appl Phys Lett 93:173301/1–173301/3
10. Kudo K, Wang DX, Iizuka M et al (1998) Schottky gate static induction transistor using copper phthalocyanine films. Thin Solid Films 331:51–54
11. Watanabe Y, Kudo K (2005) Flexible organic static induction transistors using pentacene thin films. Appl Phys Lett 87:223505/1–223505/3
12. Xue Y-B, Wang D-X (2006) Experimental analysis of operating characteristics of organic semiconductor static induction transistor. J Shanghai Univ 10:352–356
13. Fukagawa H, Watanabe Y, Kudo K, et al (2009) Ext Absr (70th Autumn Meet), Japan Society of Applied Physics, 8p-K-8 (in Japanese)
14. Lampert MA, Mark P (1970) Current injection in solids. Academic Press, New York
15. Kao KC (2004) Dielectric phenomenon in solids. Elsevier, Amsterdam
16. Weis M, Manaka T, Iwamoto M (2009) Origin of electric field distribution in organic field-effect transistor: experiment and analysis. J Appl Phys 105:24505/1–24505/7
17. Weis M, Manaka T, Iwamoto M, Effect of traps on carrier injection and transport in organic field-effect transistor, IEEJ Trans Elect Electronic Eng (in press)
18. Tamura R, Lim E, Manaka T, et al (2006) Analysis of pentacene field effect transistor as a Maxwell–Wagner effect element. J Appl Phys 100:114515/1–114515/7
19. Dimitrakopoulos CD, Purushothaman S, Kymissis J et al (1999) Low-voltage organic transistors on plastic comprising high-dielectric constant gate insulators. Science 283:822–824
20. Shockley W (1952) A unipolar "field-effect" transistor. Proceedings of the IRE 40:1365–1376
21. Silveira WR, Marohn JA (2004) Microscopic view of charge injection in an organic semiconductor. Phys Rev Lett 93:116104/1–116104/4
22. Bulucea C, Rusu A (1987) A first-order theory of the static induction transistor. Solid-State Electron 30:1227–1242
23. Wang DX, Tanaka Y, Iizuka M et al (1999) Device characteristics of organic static induction transistor using copper phthalocyanine films and al gate electrode. Jpn J Appl Phys 38:256–259
24. Dunn L, Basu D, Wang L, Dodabalapur A (2006), Organic field effect transistor mobility from transient response analysis. Appl Phys Lett 88:063507/1–063507/3
25. Basu D, Wang L, Dunn L, et al (2006) Direct measurement of carrier drift velocity and mobility in a polymer field-effect transistor. Appl Phys Lett 89:242104/1–242104/3
26. Manaka T, Lim E, Tamura R et al (2007) Direct imaging of carrier motion in organic transistors by optical second-harmonic generation. Nat Photonics 1:581–584
27. Kepler RG (1960) Charge carrier production and mobility in anthracene crystals. Phys Rev 119:1226–1229
28. Spear WE, Mort J (1963) Electron and hole transport in CdS crystals. Proc Phys Soc 81:130–140
29. Scher H, Montroll W (1975) Anomalous transit-time dispersion in amorphous solids. Phys Rev B 12:2455–2477

30. Horowitz G (2006) Organic transistors. In: Klauk H (ed) Organic electronics, Wiley-WCH, Weinheim
31. Manaka T, Liu F, Weis M, et al (2009) Mobility measurement based on visualized electric field migration in organic field-effect transistors. Appl Phys Express 2:061501/1–061501/3
32. Manaka T, Liu F, Weis M, et al (2010) Influence of traps on transient electric field and mobility evaluation in organic field-effect transistors. J Appl Phys 107:043712/1–043712/7
33. Lin J, Weis M, Taguchi D et al (2009) Carrier injection and transport in organic field-effect transistor investigated by impedance spectroscopy. Thin Solid Films 518:448–551
34. Lim E, Manaka T, Iwamoto M (2008) Analysis of pentacene field-effect transistor with contact resistance as an element of a Maxwell–Wagner effect system. J Appl Phys 104:054511/1–054511/5
35. Aswal DK, Lenfant S, Guerin D et al (2006) Self assembled monolayers on silicon for molecular electronics. Anal Chim Acta 568:84–108
36. Possanner SK, Zojer K, Pacher P et al (2009) Threshold voltage shifts in organic thin-film transistors due to self-assembled monolayers at the dielectric surface. Adv Funct Mater 19:958–967
37. Yoshita S, Tamura R, Taguchi D, et al (2009) Displacement current analysis of carrier behavior in pentacene field effect transistor with poly(vinylidene fluoride and tetrafluoroethylene) gate insulator. J Appl Phys 106:024505/1–024505/4
38. Wang SD, Minari T, Miyadera T, et al (2007) Contact-metal dependent current injection in pentacene thin-film transistors. Appl Phys Lett 91:203508/1–203508/3
39. Miyadera T, Nakayama M, Ikeda S et al (2007) Investigation of complex channel capacitance in C_{60} field effect transistor and evaluation of the effect of grain boundaries. Curr Appl Phys 7:87–91
40. Minari Y, Nemoto T, Isoda S (2004) Fabrication and characterization of single-grain organic field-effect transistor of pentacene. J Appl Phys 96:769–772
41. Diao L, Frisbie CD, Schroepfer DD, et al (2007) Electrical characterization of metal/pentacene contacts. J Appl Phys 101:14510/1–14510/8
42. Vig JR (1985) UV/ozone cleaning of surfaces. J Vac Sci Technol. A 3:1027–1034
43. Suzue Y, Manaka T, Iwamoto M (2005) Current–voltage characteristics of pentacene films: effect of UV/ozone treatment on Au electrodes. Jpn J Appl Phys 44:561–565
44. Wan A, Hwang J, Amy F et al (2005) Impact of electrode contamination on the α-NPD/Au hole injection barrier. Org Electron 6:47–54
45. Campbell IH, Rubin S, Zawodzinski TA et al (1996) Controlling Schottky energy barriers in organic electronic devices using self-assembled monolayers. Phys Rev B 54:R14321–R14324
46. Jang Y Cho JH, Kim DH et al (2007) Effects of the permanent dipoles of self-assembled monolayer-treated insulator surfaces on the field-effect mobility of a pentacene thin-film transistor. Appl Phys Lett 90:132104/1–132104/3
47. Kelley TW, Frisbie CD (2001) Gate voltage dependent resistance of a single organic semiconductor grain boundary. J Phys Chem B 105:4538–4540
48. Wang SD, Minari T, Miyadera T, et al (2008) Bias stress instability in pentacene thin film transistors: contact resistance change and channel threshold voltage shift. Appl Phys Lett 92:63305/1–63305/3
49. Necliudov PV, Shur MS, Gundlach DJ et al (2003) Contact resistance extraction in pentacene thin film transistors. Solid-State Electron 47:259–262
50. Weis M, Nakao M, Lin J et al (2009) Thermionic emission model for contact resistance in organic field-effect transistor. Thin Solid Films 518:795–798